Chemical Physics Letters 615 (2014) 124–131

Contents lists available at ScienceDirect

Chemical Physics Letters

journal homepage: www.elsevier.com/locate/cplett

FRONTIERS ARTICLE

Sum frequency spectroscopy of the hydrophobic nanodroplet/water interface: Absence of hydroxyl ion and dangling OH bond signatures

Jean-Sebastién Samson[a], Rüdiger Scheu[a], Nikolay Smolentsev[a], Steven W. Rick[b], Sylvie Roke[a,*]

[a] Laboratory for fundamental BioPhotonics (LBP), Institute of Bio-engineering (IBI), School of Engineering (STI), École Polytechnique Fédérale de Lausanne (EPFL), CH-1015 Lausanne, Switzerland
[b] Department of Chemistry, University of New Orleans, New Orleans, LA 70148, USA

ARTICLE INFO

Article history:
Received 8 September 2014
In final form 11 September 2014
Available online 2 October 2014

ABSTRACT

Vibrational sum frequency scattering measurements were performed on deuterated hexadecane oil nanodroplets dispersed in aqueous pH neutral and basic solutions. The predominant symmetry of the observed vibrational signatures was derived using nonlinear light scattering theory. The probed spectral region contains information about two distinct phenomena: The surface structure of water, and the spectral signature of surface OD^- ions. The spectral data differ from that of the planar alkane/water interface, but can be interpreted consistently by considering differences in chain orientation and molecular surface corrugation. In terms of the second phenomenon, we find that although the electrokinetic mobility increases with pH, the SF spectra do not change with increasing pH, and do not contain any evidence for the presence of interfacial hydroxyl ions. Based on expected surface charge densities, signal strength and recent literature, we conclude that a charge transfer scenario is most in accord with the present data.

1. Introduction

Liquid hydrophobic/water interactions and interfaces play a key role in biological [1] and chemical processes [2]. In biology, processes such as enzyme activity, protein folding, catalysis, and membrane formation depend on hydrophobic/water interactions [1]. In chemistry [2,3], the same holds for processes such as wetting, drug design, aerosol formation and stabilization, nanoparticle and droplet formation and stabilization, protein folding and emulsification. The structure of water at hydrophobic interfaces depends on characteristics such as charge, dielectric constant and dipole moment, as well as the molecular shape/geometry and related corrugation [4]. Understanding of these complex and multifaceted phenomena will lead to an increased understanding of water structure in the presence of ions, surfactants, proteins and other biological interfaces.

The liquid alkane/water interface functions as an ideal model system to study the structure and interactions that are relevant for the behavior of water in the presence of hydrophobes in biologically relevant systems. Since alkane/water interfaces are difficult to prepare and measurements of the molecular structure are challenging [5], only a few studies have been performed. Infrared (IR)-visible sum frequency (SF) generation is a surface sensitive method that can measure a vibrational coherent surface response of a particular vibration that is both Raman and IR active [6,7]. Sum frequency generation is thus well suited to probe the structure of the surface region. The Richmond lab [8–10] has investigated planar water/CCl_4 and water/alkane systems and concluded that the hydrogen bonds between water molecules at these interfaces are significantly weaker than at the air/water interface. Bakker and coworkers however, found from SFG studies on the same systems that the ordering of hydrogen bonded water molecules is rather enhanced [11]. Thus, few experimental studies have been performed to elucidate the water structure at the hydrophobic/liquid water interface, and from these it appears that the surface structure of water is not yet very well defined.

Apart from the multiple uncertainties surrounding the interfacial water structure, there are other controversial properties. One of the most remarkable features of the hydrophobic/water interface is that it carries a negative charge [12–17]. This negative charge has been measured on air bubbles and hydrophobic nanoparticles and droplets using pH dependent electrokinetic mobility measurements [12–14,18] or acid base titration experiments [16,19]. While the sign of the charge at neutral pH is negative, the source of

* Corresponding author.
E-mail address: sylvie.roke@epfl.ch (S. Roke).

http://dx.doi.org/10.1016/j.cplett.2014.09.034
0009-2614/

the negative charge has lately come under debate (see e.g. Refs. [18,20]). The most intuitive and long standing explanation for the negative charge of the hydrophobic/water interface is that OH^- ions from the water autoprotolysis reaction preferentially adsorb in the surface region (e.g. Refs. [14,18]). In recent years, this explanation has been tested by a search for spectroscopic signatures that are directly attributable to OH^- ions in the interfacial region. OH^- may be detected in the interfacial region by means of its 2 pπ valence excitation, using X-ray photoelectron spectroscopy (XPS) on a liquid jet. XPS is interface-sensitive over a length scale of a few nm. Using this method, OH^- ions were, however, not detected in the surface region [21]. Another direct route is the detection of a resonant second harmonic generation (SHG) signal of the optical charge transfer-to-solvent transition of interfacial OH^- ions at a wavelength of 190 nm [22,23]. Petersen et al. [23] did not detect any preferential adsorption of OH^- ions at the air/water interface. Alternatively, the OH/OD stretch vibration of OH^-/OD^- ions could be detected [24,25]. The infrared and Raman spectra of basic aqueous solutions both contain spectral features of hydroxide ions. Strongly basic solutions display a sharp vibrational frequency resonance at ~3625 cm^{-1} (~2705 cm^{-1}) for H_2O (D_2O) solutions that is absent in the pure water spectrum [25]. Hermannson et al. [25] have recently calculated that the isolated OH^- (OD^-) ion in solution is encaged by surrounding water molecules and vibrates at 3645 (2720) cm^{-1}.

Here we investigate both the structure of the liquid oil/water interface, as well as the origin of the charge of this interface. To this end, we performed vibrational sum frequency scattering measurements on deuterated hexadecane oil nanodroplets dispersed in aqueous pH neutral and basic solutions. The spectra were recorded in multiple polarization combinations. Analysis of the polarization ratios with nonlinear light scattering theory was used to assign a predominant symmetry to the observed vibrational signatures. Since the probed spectral region contains information about weakly hydrogen bonded water molecules it holds information about the water structure as well as the presence or absence of the hydroxyl signature. In terms of the water structure, the obtained spectral data differ from that obtained from the planar alkane/water interface, but can be interpreted consistently considering the likely difference in alkane chain orientation and corrugation that exist between the planar short chain alkane/water interface and the long alkane nanodroplet/water interface. In terms of the second phenomenon, the presence of hydroxyl ions, that may or may not be a source for the negative charge at the hydrophobic nanodroplet water interface, we compare electrokinetic mobility measurements with sum frequency scattering spectroscopy for increasing pH values. While the electrokinetic mobility increases drastically with pH, the SF spectra do not change with increasing pH, and do not contain any evidence for the presence of interfacial hydroxyl ions. From a discussion that includes expected surface densities of charge and expected signal strength and several mechanisms for surface charging, we conclude that a charge transfer scenario is most in accord with the present data.

In what follows, we first describe IR transmission data of our samples, which is followed by SF scattering data from the surface of the deuterated hexadecane droplets obtained at different polarizations. The spectroscopic measurements are performed in D_2O rather than H_2O, which is not expected to alter the observations. We then describe the pH dependent electrokinetic mobility data, from which we calculate the approximate amount of surface charge, and the pH dependent SF intensity and polarization ratios. This is followed by an analysis of the symmetry species of the vibrational modes that gives rise to the vibrational spectra. Finally, we discuss in separate parts the interpretation of the data in terms of the surface structure and the interpretation of the data in terms of the pH dependence and the mechanism that leads to a surface charge on the hydrophobic droplet/water interface.

2. Results

2.1. Spectral characterization of the surface region

In order to characterize the oil nanodroplet/water system, we measured transmission IR spectra of D_2O. Figure 1 shows a transmission IR spectrum of a 50 μm thick sample of the used D_2O. It can be seen that D_2O has a broad spectral absorption band that extends in the high frequency side to ~2850 cm^{-1}. Since the scattering experiments are performed in transmission geometry using a 10–1000 μm thick cuvette, the IR pulses will lose their intensity as they travel through the dispersion. The combined absorption and scattering effects [26] limit in this case the accessible spectral window to the region above ~2670 cm^{-1}. Nevertheless, this limited window can still provide us information about the interfacial vibrational modes of the part of the water molecules that have a vibrational SF active mode along the surface normal and hence the interfacial structure of water. Above 2670 cm^{-1} one expects to find water molecules with a single or no H-bond donors [27]. As an example, the dangling OD bond vibrates at 2745 cm^{-1} [11].

Figure 2 shows SFS spectra in PPP (A) and SSP (B) polarization combination for different pD values. The spectra display a sharply increasing intensity edge at ~2670 cm^{-1}, which corresponds to the strongly (bulk) adsorptive part of D_2O, with a low intensity plateau that decreases with increasing wavenumber, but extends form 2700 cm^{-1} to 2850 cm^{-1}. The signal does not contain any ~20 cm^{-1} broad features at the location of the free OD or OD^- frequencies. The sharply increasing intensity edge originates from

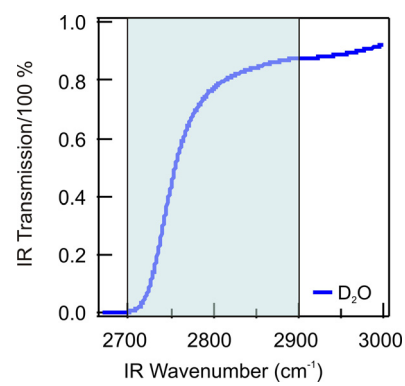

Figure 1. FTIR spectra of the D_2O used in this experiment. The optical path length of the sample cell was 50 μm. The shaded area indicates the spectral range that is accessible in the current SF scattering experiments.

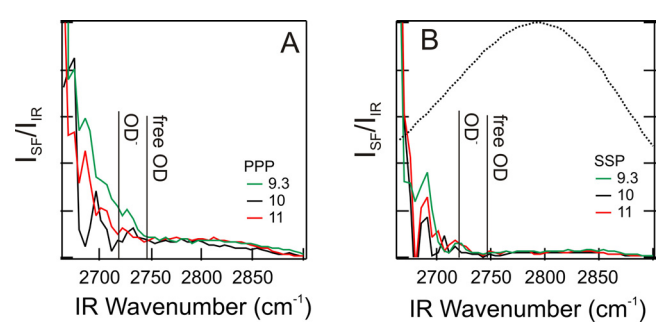

Figure 2. Surface water characterization. SFS spectra in the blue spectral part of the O—D stretch vibrational spectrum of the d_{34}-hexadecane droplet/D_2O interface, taken in PPP (A) and SSP (B) polarization for different pH values. Within the detection limit of our instrument no spectral changes are observed at different bulk pD values. The vibrational resonances of OD^- ions [25] and free OD modes [11] are indicated in the graph. The dashed line in panel B represents the envelope of the IR field. SSP (PPP) indicates a polarization combination with an S (P) polarized sum frequency beam, an S (P) polarized visible beam and a P (P) polarized IR beam.

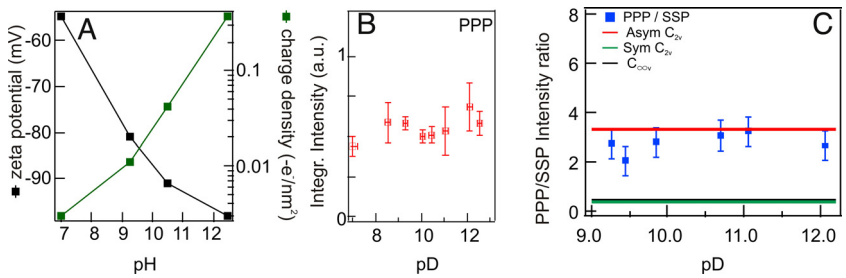

Figure 3. (A) pH dependence of the interfacial charge and water structure. Zeta potential data for 0.1 vol.% n-hexadecane droplets dispersed in water as a function of the pH of the bulk solution. The calculated charge density values are also given. (B) Integrated sum frequency intensity between 2700 and 2800 cm^{-1} as a function of solution pD for the PPP polarization combination. (C) The polarization ratio of the SF spectra, plotted as a function of pD, together with the calculated values for modes with different symmetries. The data were obtained by dividing the integrated values of the PPP and SSP intensities. The straight lines represent the calculated polarization ratios for the antisymmetric C_{2v} stretch mode (red line), the symmetric C_{2v} stretch mode (green line) and the $C_{\infty v}$ stretch mode (black line).

the normalization procedure: Dividing a small SFG intensity by the intensity of the transmitted IR pulse that has almost no intensity below 2670 cm^{-1} results in large values below 2670 cm^{-1}. No signal is present above 2850 cm^{-1}. The frequency width of the incoming IR pulse exceeds the shown spectral region and is indicated as a dashed curve in panel B. It should be noted that the actual pulse that is felt at the interface will have almost no frequency components due to absorption as shown in Figure 1. Moving the IR pulse toward lower/higher frequencies results in a reduction of the overall intensity of the plateau, but does not alter the spectral response.

2.2. pH dependence

Figure 3A shows zeta potential data for 275 nm droplets of d_{34}-hexadecane oil dispersed in water from pH neutral conditions up to pH 13. It can be seen that with increasing pH values the zeta potential decreases, so that the charge density within the slip plane increases. The data is in agreement with previously published work [14,18]. Charge densities (green points) were calculated using the generalized solution to the Poisson–Boltzmann equation for spherical particles [28]:

$$\sigma(\zeta) = \frac{2\varepsilon\varepsilon_0\kappa k_b T}{e}\left[Sinh\left(\frac{e\zeta}{2k_bT}\right) + \frac{2}{\kappa R}Tanh\left(\frac{e\zeta}{4k_bT}\right)\right] \quad (1)$$

where ζ is the zeta potential (in V), R is the particle radius, k_b is the Boltzmann constant ($k_b = 1.381 \times 10^{-23}$ J/K), T is the temperature (293 K), ε is the dielectric constant of water ($\varepsilon = 80.2$), e is the elementary electric charge (1.602×10^{-19} C), ε_0 is the permittivity of free space ($\varepsilon_0 = 8.854 \times 10^{12}$ C^2/Jm), and $\kappa = \sqrt{(ne^2/\varepsilon\varepsilon_0 k_b T)}$ is the Debye screening length with n the total number density of ions. It can be seen that with increasing pH the zeta potential decreases, so that the charge density within the slip plane increases, up to values of −0.37 charges/nm^2. For D_2O a similar graph is obtained (not shown). Figure 3B shows the integrated SF intensities for 275 nm droplets of d_{34}-hexadecane oil dispersed in heavy water from pD neutral conditions up to pD 13. The graph displays a signal that is practically constant as a function of pH within the error bar of our experiment. Figure 3C displays the intensity ratio of the PPP and SSP data obtained for various pH values. The ratio varies little in the probed pD range of 9–12.2, and has an average value of 2.7. The polarization ratio can be used to identify the predominant molecular symmetry species on the surface [29]. Although it is possible to record zeta potential data under acidic conditions, the SF experiments cannot be performed under those conditions, as the droplet stability is strongly pH/pD dependent [18]: below pH ∼5 the droplets are insufficiently stable to record SFS data.

2.3. Analysis of symmetry properties if the vibrational modes

To determine the dominating symmetry mode of the probed collection of vibrational modes, we use nonlinear light scattering theory [29]. The expected polarization ratios can be calculated for stretch modes with symmetric C_{2v} character, antisymmetric C_{2v} character, and symmetric $C_{\infty v}$ character. These three modes are representative of the purely symmetric H—O—H stretch vibration, the antisymmetric H—O—H stretch vibration, and an O—H^- or free OH stretch vibrations respectively. The hyperpolarizability values of the vibrational modes are given in Table 1. Since it is generally assumed that the hyperpolarizability values for H_2O and D_2O are comparable, we use the values for H_2O/OH^- in our model (even though the measurements are performed on D_2O) [30]. In order to calculate the polarization ratios we modified the equations of Ref. [29] to explicitly take the linear dielectric constants into account, following the procedure by Dadap et al. [31]: We replace the radial (or normal, ⊥, i.e. $\chi^{(2)}{}_{\perp\perp\perp}$, $\chi^{(2)}{}_{\perp\parallel\parallel}$, $\chi^{(2)}{}_{\parallel\perp\parallel}$ and $\chi^{(2)}{}_{\parallel\parallel\perp}$) elements of $\boldsymbol{\chi}^{(2)}$ with the $\boldsymbol{\chi}^{(2)}$ elements multiplied by the square of the refractive index of the appropriate frequency term.

Table 1 also lists the input values for the relative values of the hyperpolarizability of H_2O (Ref. [32,33]) and OH^- (Ref. [34]), the refractive index of D_2O [35], and d_{34}-hexadecane [5,36]. This procedure generates results very close to our exact nonlinear Mie scattering code [37]. For an average droplet radius of 275 nm, an experimental scattering angle (θ) of 60°, and IR/VIS opening angle of 15°, IR (VIS) wavenumbers of 2700 cm^{-1} (12 500 cm^{-1}), and the $\boldsymbol{\beta}^{(2)}$ [32–34] and refractive index values [5,36,35] as given in Table 1, we obtain the three limiting polarization ratios shown as green, red, and black lines in Figure 3C. For the symmetric stretch modes

Table 1
Refractive index and hyperpolarizability values used for the nonlinear light scattering calculations.

Refractive index (n)	SF	VIS	IR
$Re[n_{C16D34}]/Im[n_{C16D34}]$ [5,36]	1.434/0	1.43/0	1.40/0
$Re[n_{D2O}]/Im[n_{D2O}]$ [35]	1.32682/0	1.32495/0	1.101/0.08
Hyperpolarizability ($\beta^{(2)}$)	Sym H—O—H [32,33]	Asym. H—O—H [32,33]	O—H^- [34]
$\beta^{(2)}{}_{ccc}$	1	0	1
$\beta^{(2)}{}_{aac}$	0.92	0	0.54–0.75
$\beta^{(2)}{}_{aca} = \beta^{(2)}{}_{caa}$	0	1	0

the polarization ratio depends only very weakly on the molecular tilt angle (increasing by ~10% from a tilt angle of 0° to 89°). For the antisymmetric stretch mode the polarization ratio depends very strongly on the tilt angle. In this case, for increasing tilt angles (with respect to the surface normal) the polarization ratio increases from a value of 3.5 to a value of 198. As we are interested only in the polarization ratio that reproduces the measured values we have only plotted the ratio for the average molecular tilt angle that describes our data most accurately. From Figure 3C it can be seen that the measured polarization ratio of the SF signal in the spectral region between 2700 and 2800 cm^{-1} agrees best with the ratio calculated for the antisymmetric stretch mode, and not with the other two.

Having presented the SF spectral data for the hydrophobic hexadecane droplet water interface, the pH dependent electrokinetic mobility and polarization data, and having analyzed the polarization dependence, we turn to a discussion of the data. We will do this first in terms of the water structure and then in terms of the molecular origin of the electrokinetic mobility.

3. Discussion

3.1. The surface water structure

To start to understand the structural aspects of the water surface that can be derived from our spectra, we first summarize our observations. This is followed by a comparison to earlier measurements, effects of laser heating and a detailed explanation of some aspects of the surface water structure. The influence of impurities on SF scattering experiments and on reflection mode SF experiments is considered in detail in the appendix.

The spectral response observed in our data is limited to wavenumbers above 2670 cm^{-1}. As such, this comprises vibrational modes of D_2O molecules that have few hydrogen bonds [27]. Furthermore, the signature of the free OD bond, which is observed as a ~20 cm^{-1} broad peak centered at 2745 cm^{-1} at the alkane/D_2O interface [11] is not present in the spectra of Figure 2. The analysis of the polarization combination further suggests that the symmetric stretch modes are not very spectrally active, in contrast to modes with a predominantly antisymmetric character. Such a signal could originate if the water molecules that are in close proximity to the alkane surface are not protruding into the oil phase, but form an 'encaging structure' with the O—H bonds lying predominantly in the surface plane. If such a layer connects with water molecules with multiple environments, we will observe only those water molecules that have few H bonds, as these are the ones that are visible in our high frequency spectral window. The antisymmetric stretch mode is observable if water molecules orient with the symmetry axis along the surface plane. The situation is sketched in Figure 4. In order to justify this interpretation, we first evaluate some properties of the alkane/water interface.

Planar alkane/water interfaces can be created by wetting from a saturated vapor of alkanes on water. The type of alkane film that is formed depends on the wetting behavior of alkanes [38]. Continuous films are formed when short and long range interactions favor wetting, which happens for very short ($<C_4$) alkanes. Wetting is not observed when both short and long range interactions disfavor wetting ($>C_8$). In an intermediate regime (C_4–C_8) where the short range interactions favor wetting but the long range interactions do not favor wetting, a thin (1–5 nm) film is formed that coexists with thicker lenses and other surface structures [39,40]. In the intermediate regime it is likely that heterogeneous films are formed. Indeed, the microscopy image (Figure 2) of a pentane film of water of Ref. [39] shows different film thicknesses, rafts, clefts and air exposed water pockets. Such wetted alkane/water interfaces have been investigated with SFG in the polarization combination SSP by several labs. Scatena et al. [8] studied the CCl_4/H_2O interface at bulk pH values of 2.44 and 9.45. They observed that compared to the air/water interface the broad spectral band of water, which is assigned to H-bonded water molecules (3100–3500 cm^{-1}) decreases with intensity for CCl_4/H_2O. The free OH mode at 3669 cm^{-1}, also decreases in relative intensity. It is also noteworthy that spectral SF intensity is present up to 3800 cm^{-1}, for the basic pH value. Brown et al. [10] observed a constant but low intensity of the broad water band (3100–3500 cm^{-1}) and a decreasing intensity for the ~20 cm^{-1} broad dangling OH mode which vibrates at 3674 cm^{-1}. Bakker and co-workers [11] recently found that the intensity of the broad water band increases drastically when going from air/D_2O to the hexane/D_2O and heptane/D_2O interface and decreases again when the temperature is raised. They suggested that the original experiments from the Richmond lab are influenced by heating effects from the IR laser pulses that interact with the bulk water. This indeed occurs in many surface film experiments on H_2O (and in a much lesser extend on D_2O) [41]. The free OD mode (2745 cm^{-1}) also appears in the spectra but is not very different for these different interfaces. OD spectral intensity continues up to 2840 cm^{-1}.

In order to understand this difference in dangling OD intensity, we first consider the conditions and number density of the dangling OH/OD bonds on various interfaces, and then correlate this to what is known about the molecular surface structure and roughness. In addition to the alkane/water interfaces, a strong spectral signature of a free OD or OH bond is observed at the air/water [42–47] the OTS/quartz/water [48,49], and a rough superhydrophobic interface

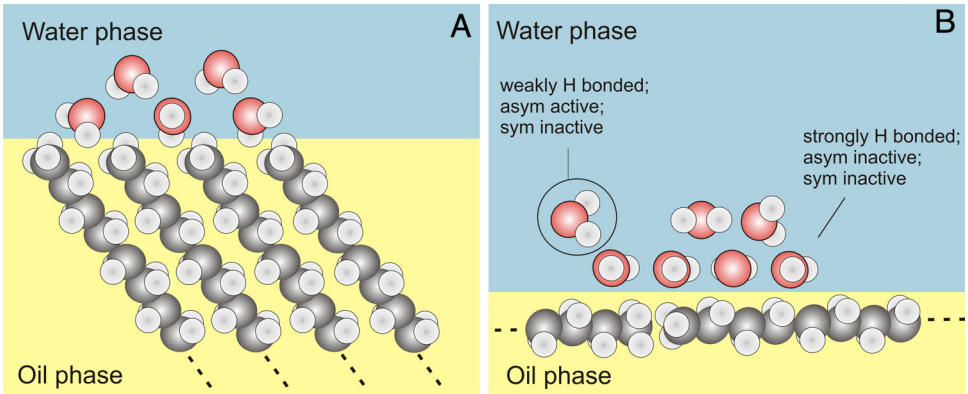

Figure 4. Schematic illustrations of possible surface structures. (A) An ordered structure of alkane chains in contact with water is shown, as commonly present in a perfectly crystalline self-assembled monolayer. Water molecules that have their dangling OH bonds in the cavities formed by the methyl groups are sketched. (B) An illustration of an alkane/water surface with more parallel oriented alkane molecules. Here, there is much less space for dangling OH bonds that have their vibrational coordinate directed along the surface normal.

[50]. On the air/water interface, it was estimated that 20% of the interface is covered with dangling OH bonds [42] which means there are ~3–4 free OH bonds per nm^2. Recent experiments by Tyrode [49] on self-assembled monolayers of octadecyltrichlorosilane on silica showed that disordered SAMs show an increase of the broad water band (3100–3500 cm^{-1}) and a relative decrease of the free OH mode. A fluidic monolayer of PNIPAM (poly-(N-isopropylacrylamide) on water, however, quenches the free OH modes [51].

The observations of Tyrode and Asanuma et al. and the trend observed by the Richmond lab (low free OH intensity for longer alkane chains) can be explained as follows: In order to facilitate a dangling OH bond, there has to be room for it, which can be made by stacking alkane chains in an ordered manner as illustrated in Figure 4A. For this geometry, free OH groups can dangle between the CH_3 groups of adjacent head groups (thus forming 'free OH pockets'). Figure 4B illustrates an alkane/water surface structure with parallel oriented alkane molecules. For this second geometry there is far less available space for free OH groups along the surface normal. Considering the geometrical constraints of both surface layers, the density of pockets for dangling OH modes is reduced by a factor determined by the chain length, which is ~16 (for hexadecane). Since the SF intensity scales with the square of the surface density the signal of the dangling OH bonds is expected to be reduced in going from the sketched structure in A to that of B by ~256, which would probably render the dangling OH modes invisible. SF scattering measurements [52] of the C—H stretch region of the alkane nanodroplet/water interface for different alkane chain lengths have recently been recorded in our laboratory. The chain length dependence and interference measurements are indeed in agreement with an average alkane chain orientation that has more CH_2 groups exposed to the water phase than CH_3 groups (i.e. a parallel chain orientation). Such a conformation might be energetically favorable considering the thermal motion of alkanes: At room temperature, the thermal energy is sufficient to translate or rotate one methyl group into the water phase. For an alkane surface with CH_3 groups in contact with the water phase, every methyl group has enough thermal energy to protrude into the water phase and create a methyl group that is surrounded by water molecules, which we refer to here as a hydrophobic cavity. For a surface with mostly CH_2 groups exposed to the water phase, only the rotational motion of a CH_3 group can result in the formation of such a hydrophobic cavity. Following this reasoning, it can be expected that longer alkane chains will likely have more parallel oriented alkanes (to reduce the amount of energetically unfavorable cavities and overall corrugation). Furthermore, as the surface area increases dramatically in a nanodroplet system compared to a planar interface the reduction of the number of unfavorable cavities is likely to become more important. The same considerations explain why the PNIPAM/water interface has no dangling OH bonds: there is no room for OH modes to dangle in. Thus, parallel alkane chains can results in a drastic reduction of free OH bonds. This would form a structure of in plane H-bonded water molecules, which are largely SF inactive. In our spectral window we would also not observe the sub-surface water molecules that have strong H bonds, but we would observe water molecules with less H bonds, of which the encircled one in Figure 4B is an example.

3.2. pH dependence and the origin of the interfacial charge

Next, we discuss our data in the context of the origin of the interfacial charge that is present on the hydrophobic droplet (or bubble) interface. We focus on two explanations, the surface adsorption of hydroxyl ions and the charge transfer model. In what follows, we summarize our observations and then consider the expectations for our SF response if the signal would be related to the presence of hydroxyl ions, taking into account detection limits and expected changes in the SF signal. Then, we consider the expectations for our SF response if the charge transfer scenario would be responsible for generating the charge. Finally, we place our results in context with recent findings.

Summarizing our data, Figure 2 shows a flat spectral response for all pH values. Figure 3 shows that although the electrokinetic mobility increases with pH, the SF intensity above 2670 cm^{-1} varies little with increasing pH. The analysis of the polarization dependence of the pH dependent SF signal agrees best with modes that are predominantly antisymmetric in character.

If the interfacial charge would originate from surface adsorbed hydroxyl ions, the SF signal of the OD^- symmetric stretch peak should be present in the spectrum, and it should be predominantly $C_{\infty v}$ symmetry in character. Hydroxyl ions in a deuterated aqueous environment vibrate around 2720 cm^{-1} [24,25] and should obey the selection rules for $C_{\infty v}$ symmetry. Published estimates of the free energy for surface adsorption range from $-45 > \Delta G > -60$ kJ/mol [13,53]. Comparing this number to that of a surfactant ion such as hexadeconoic acid or dodecylsulfate (with a $\Delta G = -30$ kJ/mol [54]) we may expect that hydroxyl ions have a stronger affinity for the surface than these surfactant ions. Based on our earlier experiments [54,55], we found that surfactant anions can be detected on the surface with both their C—H and S—O stretch modes (that have comparable SF cross-sections) from concentrations in the order of 5–10 μM (on d_{34}-hexadecane droplets in D_2O as used in this study). Since the SF cross section for the C—H modes is comparable to that of the O—D modes [56], we may expect changes in the SF signal at comparable concentrations, i.e. from pD ~9. Furthermore, based on a change in the structure of the interfacial layer, simulations of the air/basic water interface have shown that the average water dipole orientational anisotropy decreases [57], which should lead to a decrease in the overall SF spectral intensity of the water signal. Since the air/water and hydrophobic/water interface share many properties, we may expect a similar behavior for the oil/water interface. Likewise, upon increasing the ionic strength in the solution, we would expect an additional decrease in the SF intensity of the water signal, as the screening is enhanced. This decrease in SF signal has been observed in both second harmonic and SF experiments on polymer PNIPAM/water interfaces [51,58], quartz/water interfaces [59–62], and polystyrene particle/water interfaces [63,64] for various salts. The same behavior has been observed on negatively charged d_{34}-hexadecane droplets in D_2O (data not shown). Thus, if hydroxyl ions adsorb on the interface, it would be reasonable to expect a sharp peak at ~2720 cm^{-1}, with $C_{\infty v}$ characteristics, as well as an overall reduction of the intensity of surrounding OD water stretch modes.

If, however, charge transfer [65] is responsible for the electrophoretic mobility, then there must be net charge transfer across the slip plane defining the boundary between the mobile and stationary layers. Simulations using charge transfer models [65,66], or using models where charge transfer is added perturbatively [67], find that there is a layer of about 5 Å thick that has water molecules with net negative charges, on average. Beyond this layer is another layer of ~5 Å thick with on average positively charged water molecules. These two layers then tend to respond differently to an external electric field and a slip plane could possibly be established between these two layers, a few Å from the oil phase. If this distance corresponds to the slip plane, then in order for that layer to maintain its negative charge it would have to maintain a net charge transfer to its neighbors across the slip plane, as is illustrated in Figure 5.

One possible mechanism involves the charged molecules changing partners as they move in response to the field and so maintain a roughly constant number of hydrogen bonds and molecular charge. Molecule *i* has a negative charge, $-\delta q$, as a result of donating more

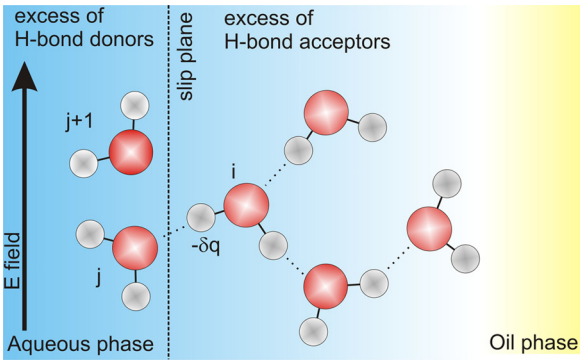

Figure 5. A charge transfer mechanism for electrophoretic mobility. The droplet moves in response to the electric field. The charge imbalance is maintained by hydrogen bonding and charge transfer across the slip plane.

H-bonds than it accepts. As the droplet moves in response to the electric field, the neutral molecules to the left of the slip plane remain stationary and the H-bond between *i* and *j* will be broken. The molecule *i* will remain negative if it can make an H-bond with molecule *j* + 1. The pH dependence suggests within this mechanism that the H-bond imbalance is influenced by excess hydroxide or hydronium ions. Since close to the interface both the positive and negative charge are increased, the water structure will be changed symmetrically on either side of the slip plane (having more H bond acceptors within the slip plane and more H bond donors outside the slip plane), which should not result in a change in the SF signal, but will result in an increasing mobility. Therefore, in this scenario we might expect that the SF signal remains constant if the pH is increased.

The data shows a spectrally broad and featureless vibrational response for the blue part of the OD spectral region. The spectral shape and intensity are both invariant to the pH within our detection limit. An increase in the spectral region at ~2720 cm^{-1} is not occurring, which disfavors the presence of hydroxyl ions. Furthermore, the symmetry (Figure 3) of the vibrational modes is predominantly antisymmetric in character which would not be in correspondence with hydroxyl ions. Thus, considering the observation and the above considerations it appears that the present data is more in favor of the charge transfer scenario.

Although our data favors the charge transfer explanation for the presence of negative charge on the hydrophobic droplet interface, there are possible scenarios in which hydroxyl ions could be present on the surface without being detectable here with SFG. If the surface vibrational frequency would be considerably lower than present spectroscopic and theoretical work suggests (i.e. below the spectral window probed here), we would not detect it. If OD^- is, for example, on average oriented with its molecular axis parallel to the plane of the interface, it would not generate any SF signal. Mundy et al. [57] calculated that the OD^- orientational distribution is not parallel (for an air/water interface). Extrapolating that this is likely the case too for the hydrophobic oil/water interface it is unlikely that all OD^- is oriented parallel with respect to the surface. Furthermore, the water signal would still be reduced in the presence of negative ions, which is not the case here. It is also possible that OD^- ions are present in many different molecular conformations as suggested by gas phase cluster experiments [68] with varying degrees of charge transfer. In this case a broad vibrational mode would result. Since the linear vibrational spectrum does exhibit a narrow band (as mentioned [25]), this seems unlikely. The present data set is therefore more in agreement with a charge transfer scenario (i.e. constant SF signal, no OD^- peak and an increase of negative charge), than with surface activity of OD^- (for which one would expect to see a spectral signature of OD^- and an overall decrease of the SF intensity). The current findings are in agreement with previous XPS studies of Aziz et al. [21] and SHG studies of Peterson et al. [23,22].

4. Conclusions

In summary, we measured the vibrational sum frequency scattering signal of the blue part of the OD spectrum of D_2O in contact with deuterated n-hexadecane nanodroplets in multiple polarization combinations and as a function of pH. The sum frequency intensity and electrokinetic mobility were measured as a function of pH from pH neutral conditions up to pH 13. While the electrokinetic mobility data displays a clear increase with pH (leading to a more negative surface charge), the SF measurements display a response that does not change within the detection limit of our system. Analysis of the polarization ratios with nonlinear light scattering theory was used to assign a predominant symmetry contribution to the observed vibrational signatures.

As the probed spectral region contains information about two distinct phenomena, namely the surface structure of water (from the signal of high frequency water OD stretch modes, such as the free or dangling OD mode), and the spectral signature of surface OD^- ions (which have recently been reported to vibrate around 2720 cm^{-1}), we have considered both effects separately.

The spectral data differs from that obtained from the planar alkane/water interface, but can be interpreted consistently considering the likely difference in alkane chain orientation and molecular corrugation that exist between the planar short chain alkane/water interface and the long alkane nanodroplet/water interface. Short chain ($<C_8$) alkanes can partially wet water and thus form heterogeneous films that may have many small cavities for free OD modes. In contrast for our long chain alkane that occupies a much larger total droplet surface area it is probably more favorable to adopt a parallel chain conformation (based on unfavorable cavity formation from thermal motion). A surface layer thus structured will have very few places available for a dangling OH mode, so that these vibrational signatures are absent from our data.

In terms of the second phenomenon, the presence of OD^- ions, that may or may not be a source for the negative charge at the hydrophobic nanodroplet/water interface, we find that although the electrokinetic mobility increases with pH, the SF spectra do not change with increasing pH, and do not contain any evidence of hydroxyl ions. From a discussion that includes expected surface densities of charge and expected signal strength and several mechanisms for surface charging, we conclude that a charge transfer scenario is more in accord with the present data. There is no evidence for surface hydroxyl ions, not from the observed vibrational modes, not from the symmetry character of the detected signal, and not form the overall (absence of) intensity change in the water spectrum as a function of pH.

5. Materials and methods

Chemicals d_{34}-Hexadecane (98% d, Cambridge Isotope), NaOH (99.99%, Sigma–Aldrich), NaOD (40 wt.% in D_2O, 99.5% d, Sigma–Aldrich), and D_2O (99.8% d, ARMAR Chemicals) were used as received. Ultra-purified, filtered and UV treated H_2O with an electrical resistance of at least 18.2 MΩ cm was obtained from a Milli-Q direct-Q-3UV system (Millipore, Inc.). Glassware was cleaned with a 3:7 H_2O_2:H_2SO_4-solution, after which it was thoroughly rinsed with ultrapure water, and subsequently D_2O if necessary.

The oil droplets were prepared by mixing 2 vol.% of d_{34}-hexadecane pH neutral D_2O, or D_2O with dissolved NaOD to reach a certain pD in a two-step process at 293 K. 4 mL of pD neutral D_2O solution was first mixed with oil using a hand-held homogenizer (TH, OMNI International) for 5 min, after which an ultrasonic bath

(Bandelin, Sonorex DK-156-BP) was used for 15 min. The pD was varied by diluting the obtained droplet solutions with D_2O solutions of a certain pD. The resultant droplets had a mean radius of 275 nm, and a polydispersity index (PDI) of ~0.2. Droplet size and zeta potential were determined using a dynamic light scattering instrument (Malvern ZS nanosizer). Although Figure 3A displays the zeta potential for hexadecane droplets in H_2O, the same measurement was performed after each SF measurement (and sample dilution from 1 vol.% to 0.1 vol.%). After correcting for the difference in viscosity between D_2O and H_2O similar zeta potential values were obtained.

Vibrational SFS spectra were measured, with equipment [69] and procedures [26] as previously described in detail using broadband infrared (IR) laser pulses centered at 2900 cm^{-1} (120 cm^{-1} FWHM bandwidth) and visible (VIS) pulses at 800 nm (12 cm^{-1} FWHM) at a repetition rate of 1 kHz. The focused laser beams were overlapped under an angle of 15° in a sample cuvette with a path length of 200 μm, which is the optimum path length for these measurments [26]. At a scattering angle of 60°, the scattered SF light was collimated with a plano-convex lens (f = 15 mm, Thorlabs LA1540-B) and then passed through two short wave pass filters (3rd Millenium, 3RD770SP and Thorlabs FES750). The SF light was spectrally dispersed with a monochromator (Shamrock 303i, Andor Technologies) and detected with an intensified CCD camera (i-Star DH742, Andor Technologies) using a gate width of 8 ns. The acquisition time of a single spectrum was 300 s. A Glan-Taylor prism (Thorlabs, GT15-B), a half-wave plate plus a polarizer (Thorlabs, LPVIS) and two BaF_2 wire grid polarizers (Thorlabs, WP25H-B) were used to control the polarization of the SF, VIS and IR beams respectively. All shown SFS spectra were normalized by the IR spectrum which was measured by SFG in reflection geometry from a z-cut quartz crystal.

Acknowledgements

Funding was received from the Julia Jacobi Foundation, and the European Research Council (ERC) under contract number 240556. SWR would like to acknowledge support from the National Science Foundation under contract number CHE-1301072.

Appendix A.

This appendix contains a description of the effects of intrinsic impurities in the used chemicals, and provides a comparison between surface experiments on planar and droplet interfaces.

A.1. Impurities

The presence of chemical impurities at the interface, caused by the inherent purity restrictions to available chemicals, can be a source of signal. For example, a 1 mL 1 mM solution of a 99.5% pure chemical may contain enough impurity molecules to cover 15–30 cm^2 of surface area (assuming a worst case scenario that all impurities are surface active and that the molecular area is 50–100 $Å^2$). Typical planar or reflection mode SFG measurements have a probing area of $\sim 1 \times 10^{-2}$ mm^2, and if they are performed in (e.g.) a Langmuir trough, the liquid volume and surface area are respectively 18–336 mL and 150–841 cm^2 [70]. Under worst case scenario conditions the Langmuir trough surface will be fully covered with impurities. To be absolutely sure that impurities do not cover more than 1% of the available surface area, chemicals with a purity of at least 99.9995% are therefore needed, which are not always available. Table 2 summarizes the result of this simple computation.

Table 2
Available interfacial area, volume, and maximum possible interfacial coverage for a hypothetical impurity molecule with a projected surface are of 1 nm^2 impurity for a small Langmuir trough and a nanodroplet system.

Parameters	Small Langmuir trough	Nanodroplets
Liquid volume (mL)	18	4
Total interfacial area (cm^2)	150	11,936
Droplet radius (nm)	–	100
Volume fraction of droplets (%)	–	1
Interfacial coverage of impurity		
Purity: 99.5%	>100% (360%)	1%
Purity: 99.95%	36%	0.1%
Purity: 99.995%	3.6%	0.01%
Purity: 99.9995%	0.36%	0.001%

This restriction is much reduced in nonlinear light scattering experiments performed on a nanodroplet system [26]: A nanodroplet dispersion can be prepared in situ using only a small volumes of chemicals. A 4 mL 4 vol.% nanodroplet dispersion of droplets with a radius of 100 nm contains ~12,000 cm^2 of surface area. For the above worst case scenario, if this solution contains 1 mM of a 99.5% pure chemical, only 1% of the available surface area can at most be covered with impurity molecules, even if all impurity molecules adsorb on the surface (i.e. irrespective of the chemical equilibrium). The hexadecane used in our study has been tested before for impurities in the organic phase [55] and we concluded that 97% of the droplet/water interface can be considered as pure (with the remaining 3% resulting from the detection limit of our system).

References

1 P. Ball, Chem. Rev. 108 (2008) 74.
2 J.N. Israelachvili, Intermolecular and Surface Forces, Academic Press, London, 1991.
3 Y.S. Jung, R.A. Marcus, J. Am. Chem. Soc. 129 (2007) 5492.
4 L.R. Pratt, A. Pohorille, Chem. Rev. 102 (2002) 2671.
5 M.M. Knock, G.R. Bell, E.K. Hill, H.J. Turner, C.D. Bain, J. Phys. Chem. B 107 (2003) 10801.
6 A.L. Harris, C.E.D. Chidsey, N.J. Levinos, D.N. Loiacona, Chem. Phys. Lett. 141 (1987) 350.
7 P. Guyot-Sionnest, J.H. Hunt, Y.R. Shen, Phys. Rev. Lett. 59 (1987) 1597.
8 L.F. Scatena, M.G. Brown, G.L. Richmond, Science 292 (2001) 908.
9 L.F. Scatena, G.L. Richmond, J. Phys. Chem. B 105 (2001) 11240.
10 M. Brown, D. Walker, E. Raymond, G. Richmond, J. Phys. Chem. B 107 (2003) 237.
11 S. Strazdaite, J. Versluis, E.H.G. Backus, H.J. Bakker, J. Chem. Phys. 140 (2014).
12 A. Graciaa, G. Morel, P. Saulner, J. Lachaise, R. Schechter, J. Colloid Interface Sci. 172 (1995) 131.
13 K.G. Marinova, R.G. Alargova, N.D. Denkov, O.D. Velev, D.N. Petsev, I.B. Ivanov, R.P. Borwankar, Langmuir 12 (1996) 2045.
14 J.K. Beattie, A.M. Djerdjev, Angew. Chem. Int. Ed. 43 (2004) 3568.
15 J.K. Beattie, A.M. Djerdjev, G. Warr, Faraday Discuss. 141 (2009) 31.
16 H. Mishra, S. Enami, R.J. Nielsen, L.A. Stewart, M.R. Hoffmann, W.A. Goddard, A.J. Colussi, Proc. Natl. Acad. Sci. U. S. A. 109 (2012) 18679.
17 R. Zimmermann, U. Freudenberg, R. Schweiss, D. Kuttner, C. Werner, Curr. Opin. Colloid Interface Sci. 15 (2010) 196.
18 P. Creux, J. Lachaise, A. Graciaa, J. Beattie, A. Djerdjev, J. Phys. Chem. B 113 (2009) 14146.
19 S. Yamaguchi, K. Bhattacharyya, T. Tahara, J. Phys. Chem. C 115 (2011) 4168.
20 R. Vacha, V. Buch, A. Milet, J.P. Devlind, P. Jungwirth, Phys. Chem. Chem. Phys. 9 (2007) 4736.
21 E.F. Aziz, N. Ottosson, M. Faubel, I.F. Hertel, B. Winter, Nature 455 (2008) 89.
22 P.B. Petersen, R.J. Saykally, J. Phys. Chem. B 109 (2005) 7976.
23 P.B. Petersen, R.J. Saykally, Chem. Phys. Lett. 458 (2008) 255.
24 N.B. Librovich, V.P. Sakun, N.D. Sokolov, Chem. Phys. 39 (1979) 351.
25 K. Hermansson, P.A. Bopp, D. Spangberg, L. Pejov, I. Bako, P.D. Mitev, Chem. Phys. Lett. 514 (2011) 1.
26 H.B. de Aguiar, J.S. Samson, S. Roke, Chem. Phys. Lett. 512 (2011) 76.
27 B.M. Auer, J.L. Skinner, J. Chem. Phys. 129 (2008).
28 R.J. Hunter, Zeta Potential in Colloid Science, Academic Press, Sidney, 1981.
29 A.G.F. de Beer, S. Roke, J. Chem. Phys. 132 (2010) 234702.
30 D.P. Shelton, J. Chem. Phys. 137 (2012) 044312.
31 J.I. Dadap, J. Shan, K.B. Eisenthal, T.F. Heinz, Phys. Rev. Lett. 83 (1999) 4045.
32 W.K. Zhang, D.S. Zheng, Y.Y. Xu, H.T. Bian, Y. Guo, H.F. Wang, J. Chem. Phys. 123 (2005).

33 D.N. Nikogosyan, Properties of Optical and Laser-related Materials: A Handbook, John-Wiley sons, New York, 1997.
34 D.P. Chong, S.R. Langhoff, J. Chem. Phys. 93 (1990) 570.
35 J.E. Bertie, M.K. Ahmed, H.H. Eysel, J. Phys. Chem. 93 (1989) 2210.
36 K.M. Wilkinson, L. Qunfang, C.D. Bain, Soft Matter 2 (2006) 66.
37 A.G.F. de Beer, S. Roke, Phys. Rev. B 79 (2009) 155420.
38 K. Ragil, D. Bonn, D. Broseta, J. Indekeu, F. Kalaydjian, J. Meunier, J. Petrol. Sci. Eng. 20 (1998) 177.
39 C. Delcerro, G.J. Jameson, J. Colloid Interface Sci. 78 (1980) 362.
40 E. Bertrand, D. Bonn, D. Broseta, H. Dobbs, J.O. Indekeu, J. Meunier, K. Ragil, N. Shahidzadeh, J. Petrol. Sci. Eng. 33 (2002) 217.
41 E.H.G. Backus, D. Bonn, S. Cantin, S. Roke, M. Bonn, J. Phys. Chem. B 116 (2012) 2703.
42 Q. Du, R. Superfine, E. Freysz, Y.R. Shen, Phys. Rev. Lett. 70 (1993) 2313.
43 M.J. Shultz, C. Schnitzer, D. Simonelli, S. Baldelli, Int. Rev. Phys. Chem. 19 (2000) 123.
44 M. Sovago, R.K. Campen, H.J. Bakker, M. Bonn, Chem. Phys. Lett. 470 (2009) 7.
45 A.M. Jubb, W. Hua, H.C. Allen, Annu. Rev. Phys. Chem. 63 (2012) 107.
46 S. Nihonyanagi, J.A. Mondal, S. Yamaguchi, T. Tahara, Annu. Rev. Phys. Chem. 64 (2013) 579.
47 I.V. Stiopkin, C. Weeraman, P.A. Pieniazek, F.Y. Shalhout, J.L. Skinner, A.V. Benderskii, Nature 474 (2011) 192.
48 S. Ye, S. Nihonyanagi, K. Uosaki, Phys. Chem. Chem. Phys. 3 (2001) 3463.
49 E. Tyrode, J.F.D. Liljeblad, J. Phys. Chem. C 117 (2013) 1780.
50 H. Asanuma, H. Noguchi, K. Uosaki, H.Z. Yu, J. Phys. Chem. C 113 (2009) 21155.
51 X. Chen, T. Yang, S. Kataoka, P.S. Cremer, J. Am. Chem. Soc. 129 (2007) 12272.
52 H.B. de Aguiar, M.L. Strader, A.G.F. de Beer, S. Roke, J. Phys. Chem. B 115 (2011) 2970.
53 C.S. Tian, Y.R. Shen, Proc. Nat. Acad. Sci. 106 (2009) 15148.
54 H.B. de Aguiar, A.G.F. de Beer, M.L. Strader, S. Roke, J. Am. Chem. Soc. 132 (2010) 2122.
55 K.C. Jena, Scheu, R. Roke, S. Angew, Chem. Int. Ed. 51 (2012) 12938.
56 M. Sovago, E. Vartianen, M. Bonn, J. Chem. Phys. 131 (2009) 161107.
57 C.J. Mundy, I.F.W. Kuo, M.E. Tuckerman, H.S. Lee, D.J. Tobias, Chem. Phys. Lett. 481 (2009) 2.
58 M.C. Gurau, S.M. Lim, E.T. Castellana, F. Albertorio, S. Kataoka, P.S. Cremer, J. Am. Chem. Soc. 126 (2004) 10522.
59 F.M. Geiger, Annu. Rev. Phys. Chem. 60 (2009) 61.
60 K.C. Jena, P.A. Covert, D.K. Hore, J. Phys. Chem. Lett. 2 (2011) 1056.
61 S. Ong, X. Zhao, K.B. Eisenthal, Chem. Phys. Lett. 191 (1992) 327.
62 M.S. Azam, C.N. Weeraman, J.M. Gibbs-Davis, J. Phys. Chem. Lett. 3 (2012) 1269.
63 K.B. Eisenthal, Method for determining surface properties of microparticles, 2000.
64 B. Schürer, S. Wunderlich, C. Sauerbeck, U. Peschel, W. Peukert, Phys. Rev. B 82 (2010) 241404.
65 R. Vacha, S.W. Rick, P. Jungwirth, A.G.F. de Beer, H.B. de Aguiar, J.S. Samson, S. Roke, J. Am. Chem. Soc. 133 (2011) 10204.
66 C.D. Wick, A.J. Lee, S.W. Rick, J. Chem. Phys. 137 (2012).
67 R. Vacha, O. Marsalek, A.P. Willard, D.J. Bonthuis, R.R. Netz, P. Jungwirth, J. Phys. Chem. Lett. 3 (2012) 107.
68 W.H. Robertson, E.G. Diken, E.A. Price, J.W. Shin, M.A. Johnson, Science 299 (2003) 1367.
69 A.B. Sugiharto, C.M. Johnson, H.B. de Aguiar, L. Aloatti, S. Roke, Appl. Phys. B 91 (2008) 315.
70 http://www.biolinscientific.com/product/langmuir-troughs-langmuir-blodgett-troughs/.

Jean-Sebastién Samson studied physics at Denis Diderot University (Paris) and Institut d'Optique (Orsay). He worked during his master thesis on far-infrared OPO at Thales TRT, and received his doctorate in physical chemistry in the team of Martina Havenith at University of Bochum in far-infrared near-field microscopy. After a post-doctoral stay in the group of Sylvie Roke (Max-Planck-Institut for Intelligent Systems, Stuttgart and EPFL) focused on sum-frequency spectroscopy, he moved to Karl Storz GmbH where he develops endoscops and different optical systems.

Rüdiger Scheu received his Diploma in Physics from the University of Konstanz where he worked in the field of Ultrafast THz Optics. In 2010, he joined the group of Sylvie Roke at the Max-Planck-Institute for Metal Physics in Stuttgart (Germany) with whom he moved to the École Polytechnique Fédérale de Lausanne (EPFL) in Switzerland. Here he received his PhD for his work employing Nonlinear Optical Methods to study specific ion effects at hydrophobic, nanoscopic interfaces.

Nikolay Smolentsev received a BSc and MSc degree with honor in physics from Southern Federal University, Rostov-on-Don, Russia. He is currently pursuing a PhD in photonics at the École Polytechnique Fédérale de Lausanne (EPFL), Switzerland, working under supervision of Prof. Sylvie Roke on nonlinear light scattering and spectroscopy of aqueous interfaces.

Steven W. Rick received his PhD in chemistry from the University of California, Berkeley. This was followed by postdoctoral positions at Brown and Columbia Universities and a staff scientist position at the National Cancer Institute in Maryland. He is currently University Research Professor at the University of New Orleans. The Rick research group uses computational methods to study aqueous and non-aqueous solutions, proteins and other polymeric materials.

Sylvie Roke obtained BSc and MSc degrees with highest honors in chemistry (1995–2000) and physics (1997–2000) from Utrecht University, and a PhD degree in natural sciences from Leiden University (2004, highest honors). In 2005, she was awarded an independent Research Group Leader position from the Max-Planck Society. In 2011, she moved to EPFL where she holds the Juli Jacobi chair in photomedicine. She received the Minerva Prize (2006), the Hertha Sponer Prize (2008) an ERC Starting Grant (2009), and an ERC Consolidator Grant (2014). Her research is focused on understanding aqueous systems, interfaces, nonlinear optics, soft matter, and biological systems.